Effect of Preheating and Water Cooling on the Performance of Friction-Stir-Welded Aviation-Grade Aluminum Alloy Joints

Shubham Verma, Meenu Gupta, and Joy Prakash Misra

(Submitted September 12, 2018; in revised form February 13, 2019; published online July 3, 2019)

This paper examined the effect of preheating and water cooling on the thermal, mechanical, metallurgical, and texture properties of friction-stir-welded AA6082. Joints are fabricated under different preheating (FSW-P) and water cooling (FSW-C) conditions. The experimental outcomes indicate that the preheating and water cooling enhance the mechanical properties of the joint. The maximum tensile strength of 295 MPa is obtained for FSW-P1. It is also observed that preheating has more impact on microhardness. Microstructural analysis using optical microscope and electron backscatter diffraction analysis indicated that FSW produced fine equiaxed grains in the nugget zone due to dynamic recrystallization. Texture analysis shows that finer grain grains are obtained under preheating and water cooling conditions. The minimum grain size of 5.3 µm is obtained under FSW-P1. X-ray diffraction analysis shows that Mg_2Si phase in nugget zone that is an indication of dissolution and formation of strengthening precipitates. Fracture analysis indicates that preheating also improves the ductility of the joint.

1. Introduction

Aviation industries are moving toward aluminum alloys specially 6xxx series (AA6061, AA6063, AA6082) for high-performance structural applications owing to its properties, namely highly formability, excellent corrosion resistance, and high strength-to-weight ratio. Recently, AA6061 and AA6063 are replaced by AA6082, as it possesses comparatively higher strength owing to presence of manganese that controls the grain structure. However, joining of this alloy by fusion welding techniques is found difficult owing to its low melting point. In addition, defects like porosity, distortion, oxidation, shrinkage, etc., are observed during fusion welding (Ref 1). Contrarily since last decade, FSW, a solid-state joining technique, is emerged as one of the best techniques to join low melting point alloys, namely aluminum alloys and copper alloys. It is free of filler and shielding gases, and hence, it is treated as green technology (Ref 2, 3). In FSW, a continuously rotated cylindrical shouldered non-consumable tool with a pin is used to join two faying surfaces. The relative motion (*mechanical stirring*) between workpiece and pin generates frictional heat to produce plasticized region at the adjacent faces. This plasticized region solidifies, and joining occurs. It is reported that application of FSW in spacecraft manufacturing increases joint strength by 30-50% and manufacturing time reduces from 23 days to 6 days with up to 60% cost saving (Ref 4).

Till date, a number of researchers have been carried out experimental investigation on FSW of aluminum alloys. Researchers attempted to enhance the mechanical and metallurgical properties of FSW joints by either varying the tool geometry or process conditions. In 2015, Dawood et al. (Ref 5) attempted to improve the mechanical and metallurgical properties of FSW AA6063 joints by varying pin geometry. It is reported that triangular pin provides better result. Trueba et al. (Ref 6) examined the effect of tool shoulder geometry on mechanical properties of AA6061 joint. It is observed that tool shoulder with raised spiral design produces higher strength joint. Heidarzadeh et al. (Ref 7) employed response surface methodology for conducting FSW experiments on AA6061 plates. It is reported that welding joint fabricated at rotational speed of 920 rpm, feed of 78 mm/min, and axial force of 7.2 kN produced higher strength joint. In, 2008 by investigating FSW of AA6082, Cavaliere et al. (Ref 8) reported the characteristics of FSW AA6082 joint by varying the welding speed in the range of 40-460 mm/min. It is concluded that joint fabricated in range of 40-165 mm/min shows strong variation in nugget zone grain size. Gopi and Manonmani (Ref 9) investigated the effect of pin profiles on FSW of AA6082. It is observed that pentagon pin profile produces higher strength joint. Recently, few studies report the application of preheating of workpiece and water cooling as an alternative solution to enhance the joint properties (Ref 10-12). Preheating softens the materials and increases the flow of materials in the stir zone. Thus, it reduces the welding forces and enhances efficiency. Past literature reports that joint strength in FSW with preheating increases 8% as compared to conventional FSW. Preheating enhances the material flow and marginal modification in deformation behavior; increases hardness of nugget zone. Thermal stresses also increase owing to presence of additional heat in HAZ. In case of FSW of dissimilar metals, preheating increases material flow in SZ and decreases void formation.

Shubham Verma, Meenu Gupta, and **Joy Prakash Misra,** Department of Mechanical Engineering, National Institute of Technology Kurukshetra, Kurukshetra, India. Contact e-mails: shubham_6140005@nitkkr.ac.in and shubham6140005@gmail.com.

Yaduwanshi et al. (Ref 12) investigated the effect of preheating during FSW of dissimilar metals and found that the developed joints are free from void defects. It results in joints with enhanced tensile and bending strength. Furthermore, additional heat reduces friction between tool and workpiece; results in low tool wear and longer tool life (Ref 13). On the other hand, water cooling increases yield strength and minimizes residual stresses. Water cooling avoids the formation of unwanted particles concentration on grain boundary, resulting in minimization of residual stresses. This process also helps in precipitation. It results in fine dispersion of particles, and compound leading to enhancement in tensile strength (Ref 14). Lui et al. (Ref 15) employed preheating for FSW of dissimilar aluminum plates and observed enhanced tensile strength.

Hence, it is evident that past research works focused on changes in mechanical and metallurgical behavior of joints mainly with varying process conditions and tool geometry. The studies lack the investigation on effect of preheating and water cooling on joint behavior during FSW of AA6082. In current research, it is attempted to study the effect of preheating and water cooling on mechanical and metallurgical behavior of AA6082 FSW joints. In addition, thermal analysis and EBSD analysis of joints produced in preheating and water cooling conditions have been carried out. Study of thermal cycle is crucial to evaluate the quality of weld. In FSW, heat is generated owing to friction between tool and workpiece. It improves the metal flow during the process and makes the transverse movement easier. If this frictional heat is too low, tool will experience hindrance in transverse movement resulting in tool breakage. In contrast, if it is too high, sticking of material to pin and shoulder will be occurred. It results in larger grain-size microstructure. Beside this, EBSD analysis conveys concept of deformation phenomenon during FSW. It consists of idea of grain size, misorientation angle, and grain boundaries (high angle and low angle). In present work, EBSD analysis has been employed to study the grain structure of nugget zone and thus joint characteristics. Furthermore, fractography of FSW joints has been executed to study the tensile fracture behavior. Further examination of the texture development in the nugget zone is also carried out by x-ray diffraction (XRD). The measurements were carried out by a diffractometer (model: Bruker, D8 Advance, Billerica, MA, USA) using CuKα (λ = 1.5406 A) radiation with an acceleration voltage of 40 kV.

2. Experimentation

2.1 Workpiece and Tool Geometry

In this investigation, 6.35 mm AA 6082-T6 plates are selected for experimentation. The EDX analysis is performed to scrutinize the phases present in AA6082 (Fig. 1). The plates are cut into 100 mm × 75 mm × 6.35 mm from another plate of dimension 320 mm × 320 mm × 6.35 mm. After that, faying surface of these plates is machined on a vertical milling machine to avoid the mismatching of the surfaces during welding. A tool of H13 material with a cylindrical threaded pin (6 mm in diameter and 6.1 mm in length) and concave shoulder (8° concave, 20 mm in diameter) is fabricated to accomplish the FSW. The dimensions and photographic view of developed tool are shown in Fig. 1(b) and (c).
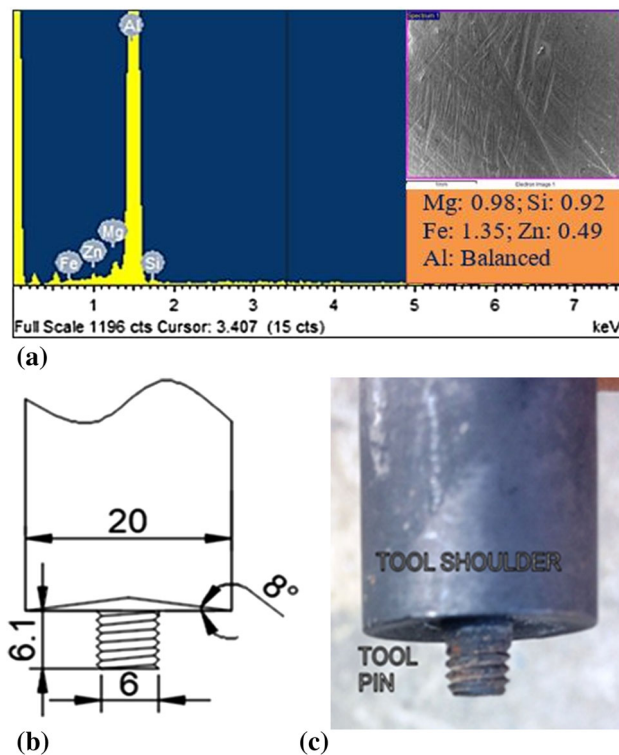

Fig. 1 (a) EDX analysis of AA6082; (b) schematic diagram of tool (dimensions are in mm); and (c) fabricated tool

2.2 Experimentation

A vertical milling machine is modified to conduct the experiments by developing special fixture (shown in Fig. 2). Joints are fabricated at constant rotational speed of 2000 rpm, feed rate of 60 mm/min, tilt angle of 2°, and dwell time of 30 s (*obtained from pilot experiments*) under preheating and water cooling conditions. For preheating, the electro-thermal-filament-based heating system with temperature regulator is developed (shown in Fig. 2(a). For water cooling, water is supplied continuously through coolant system as shown in Fig. 2(b). In current research, experimentation has been conducted for three different preheating and water cooling conditions. Table 1 presents the experimental conditions and process parameters for current research.

2.3 Thermocouple Layout

Eight thermocouples of *K* type are used for measuring the temperature at different locations on both sides. These thermocouples are connected to the instrument named as UNILOG for data acquisition. It consists of two units: one is used for data recording on excel sheet named universal process data recorder and second is used for transferring the data from thermocouples to data recorder named as channel interface module. For each experimental condition, thermocouples are fixed at the center of the plate; four thermocouples are placed on retreating side (RS) and four are placed on advancing side (AS). First thermocouple on each side is placed at a distance of 14.5 mm from centerline to prevent the crushing of thermocouples during the process. After that, remaining thermocouples are placed at equal pitch of 10 mm. The layout of thermocouples is depicted in Fig. 2(c) and (d). Thermocouples used in this study are L shaped with tip diameter of 3 mm. Therefore, a blind hole of 3 mm diameter is
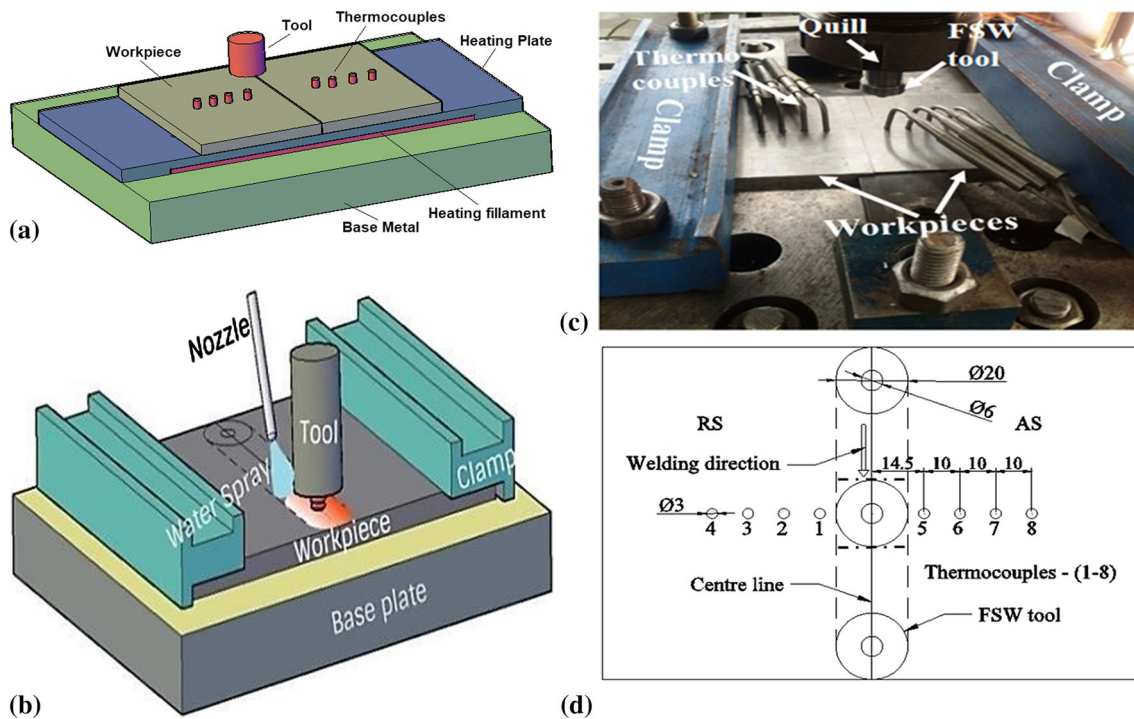
Fig. 2 (a) Schematic diagram of preheating system; (b) schematic diagram for water cooling; (c) arrangement of thermocouples; and (d) position of the thermocouples inside the workpiece

Table 1 Experimental conditions and process parameters

Experimentation	Designation	Conditions		Process parameters
Air-welded	FSW-A	Atmospheric air		Rotational Speed: 2000 rpm
Preheating (FSW-P)	FSW-P1	Plate temperature	100 °C	Feed rate: 60 mm/min
	FSW-P2		125 °C	Tilt angle: 2°
	FSW-P3		150 °C	Dwell Time: 30 s
Water cooling (FSW-C)	FSW-C1	Water temperature	2 °C	Plunge Depth: 2 mm
	FSW-C2		22 °C	
	FSW-C3		65 °C	

drilled into the workpiece plates for inserting the thermocouples. The hole is drilled up to 5 mm in depth as the plate thickness is 6.35 mm to prevent the contact between thermocouple tip and base plate.

2.4 Mechanical and Microhardness Testing

From the welded plates, tensile specimens are cut in perpendicular to welding direction as shown in Fig. 3(a). Tensile specimens are prepared as per ASTM E8M-04. Initially, the rectangular strips (150 mm × 12 mm × 6.35 mm) are cut from welded sample using power hacksaw. After that, these strips are converted into tensile specimen utilizing end-mill-cutter. The detailed dimension of specimens is illustrated in Fig. 3(b). Tensile testing has been conducted in UTM (*Make: Bangalore Integrated System Solutions*) for evaluating the tensile strength and percentage elongation of FSW joints (*Strain rate*—2 mm/min). The specimens for microhardness testing are cut into rectangular strips (22 mm × 6 mm × 6.35 mm) from welded plates from the centerline as shown in Fig. 3(c). After that, emery papers of 400, 600, 800, 1000,

1200, 1500, and 2000 grit size are employed for maintaining uniformity in top and bottom surfaces of specimens to avoid error during measurement. Subsequently, cloth polishing is tried for making more reflective and scratch-free surface. Finally, these samples are analyzed by Vickers microhardness at 200 g load.

2.5 Microstructural Observation and Fractography

The sample preparation for metallurgical analysis is same as of microhardness. After cloth polishing, samples are chemically etched with Keller's reagent, which is a solution of 95 ml distilled water, 2.5 ml HNO₃, 1.5 ml HCL, and 1 ml HF. After that, samples are analyzed at macroscopic and microscopic level using optical microscope (*Make: Conation Technologies*) and SEM (*Make: JEOL Ltd.*), respectively. Optical microscope is employed to visualize the different welding zones. Finally, the samples of FSW-A, FSW-P1, and FSW-C3 conditions are analyzed by SEM with EBSD attachment for measuring grain size in nugget zone. The fracture surfaces of tensile specimens are analyzed using SEM for fractography analysis.
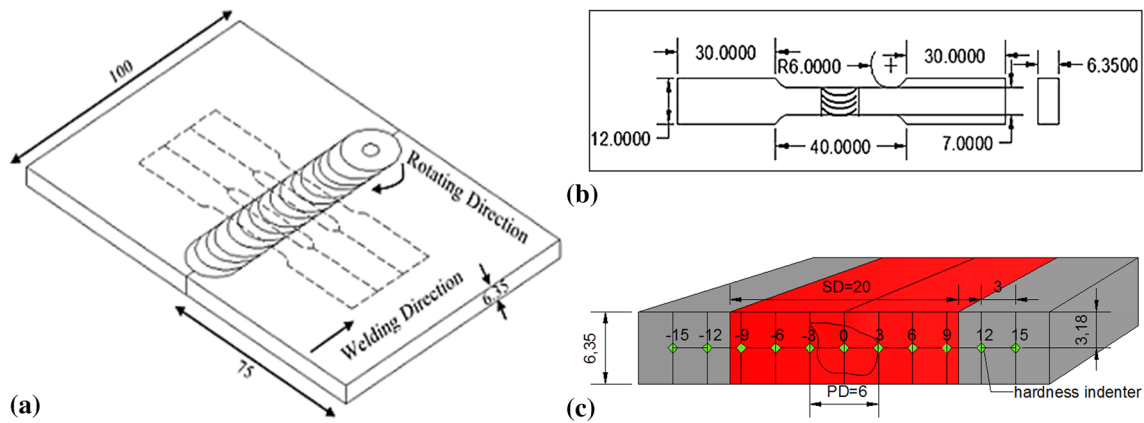
Fig. 3 (a) and (b) Schematic diagrams for tensile testing; (c) schematic diagram of different location for measuring microhardness

3. Result and Discussion

3.1 Thermal Analysis

The temperature distribution in advancing side (AS) and retreating side (RS) during FSW is illustrated using thermal cycle plot. Figure 4 presents the thermal cycle plots under different welding conditions presented in Table 1. The thermal cycle of FSW is completed in four stages: plunge time (PLT), dwell time (DT), process time (PT), and pullout time (POT). In plunge time, pin plunges between the faying surfaces of the plates. During dwell time, tool is kept constantly rotating at starting point without any transverse movement after plunging into faying surfaces. The time taken to complete the welding process is termed as process time, while the time taken to pullout the pin after completion of process is labeled as pullout time. These stages are presented in Fig. 4(a). It is evident that for present research plunge time is 20 s, dwell time is 30 s, process time is 80 s, and pullout time is 20 s. In FSW, heat input is a function of friction between the tool and workpiece. It results in temperature rise in stir zone (SZ). This heat significantly affects the mechanical and metallurgical properties of the fabricated joint of heat-treatable alloys (Ref 11, 16). Therefore, thermal cycle plays a crucial role in the quality of weld. It is observed from Fig. 4 that AS temperature is higher than RS. It confirms non-symmetrical heat generation during the process. This is happened owing to movement of material from AS to RS by rotating pin. Figure 4(a) presents the temperature distribution during simple FSW accomplished under atmospheric condition. It is observed from the diagram that before PLT process temperature is 25 °C and it starts increasing during plunging. This temperature rise continues till before POT. The maximum temperature is obtained just before ending of PT. Figure 4(b), (c), and (d) illustrates the temperature distribution of FSW under preheating conditions. It is clearly visible from Fig. 4(b), (c), and (d) that initial temperatures are higher than both FSW under atmospheric condition and FSW with water cooling. It is owing to the additional heat input during preheating. Consequently, the maximum temperature obtained during this condition is higher than other two cases. Figure 4(e), (f), and (g) presents the temperature distribution of FSW with water cooling. The initial temperature is similar to FSW under atmospheric condition, although the maximum temperature obtained during the process is comparatively lesser than preheating and atmospheric condition.

Moreover, there is a sudden drop of temperature after PT as shown in Fig. 4(e), (f), and (g). It is attributed to the combined effect of water cooling and lack of frictional heat input after PT. Peak temperatures on AS and RS for different welding conditions are illustrated in Fig. 5. It is observed that highest peak temperature of 360 °C is obtained at AS for FSW-P3 condition.

3.2 Tensile Testing

Table 2 reveals the outcomes of present study. Maximum tensile strength of parent metal is observed as 310 MPa. In FSW-A, the tensile strength of joint is obtained 260 MPa, which is 83% of parent metal strength. This decrement in the strength is owing to low density and dissolution of precipitates in NZ owing to dynamic recrystallization (Ref 17). This degradation of mechanical properties is tried to improve by preheating and water cooling. The tensile properties of joints under different welding conditions are shown in Fig. 6. The stress vs. strain relationship is shown in Fig. 7. It is evident from Table 2 that in case of preheating, maximum tensile strength is obtained for FSW-P1; 13.5% improvement over FSW-A. In case of water cooling, maximum tensile strength is obtained for FSW-C3; 4% improvement over FSW-A.

In case of preheating condition, the additional heat input helps in softening of material in nugget zone; enhances the mixing of material. It results in improved weld behavior. In addition, preheating helps in reduction of plunge forces and friction between tool and workpiece resulting in longer tool life (Ref 18). It is observed that the tensile strength is increased initially at 100 °C, but drops progressively at 125 °C and 150 °C (Fig. 6). At 100 °C and 125 °C, strength is increased by 13% and 10% over FSW-A, respectively. In contrast, it is decreased by 4% at 150 °C. At low temperature (100 °C), the strength is high owing to presence of strengthening particles in the structure, but with further increase in preheating temperature up to 125 °C these strengthening particles are started transform into coarse and rod shape particles that resulted in degradation of mechanical strength. At 150 °C, the heat input increases. As a result of it, transformation of strengthening particles into coarse and rod shape particles increases. It results in further degradation of mechanical strength.

Alternatively, water cooling helps in undesirable concentration of alloying elements on the grain boundary, which result in uniformly dispersion of second-phase particles (Ref 14).
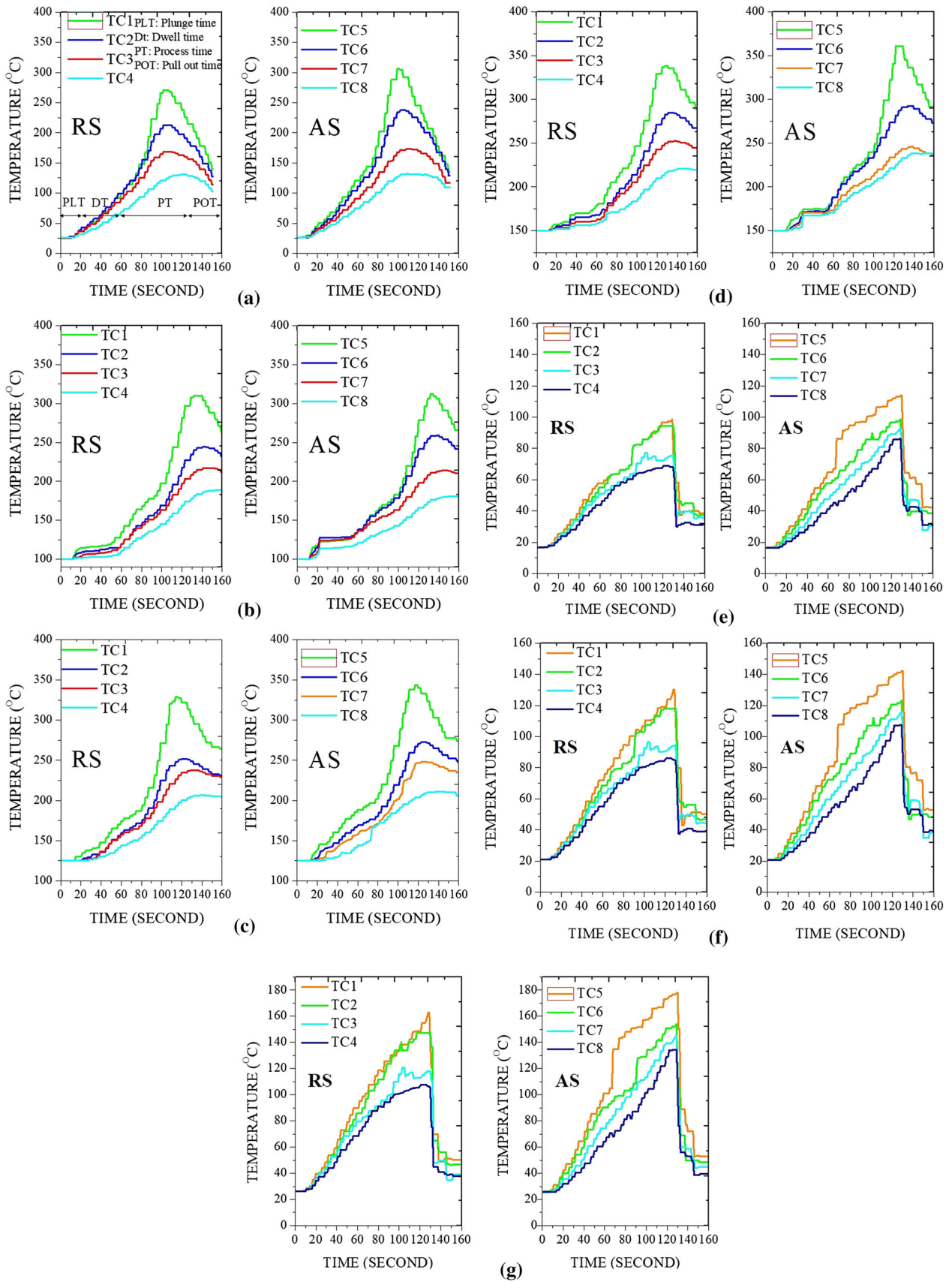
Fig. 4 Temperature distribution during FSW under (a) atmospheric (FSW-A); (b), (c), and (d) preheating (FSW-P1/FSW-P2/FSW-P3, respectively); and (e), (f), and (g) water cooling (FSW-C1/FSW-C2/FSW-C3, respectively) condition
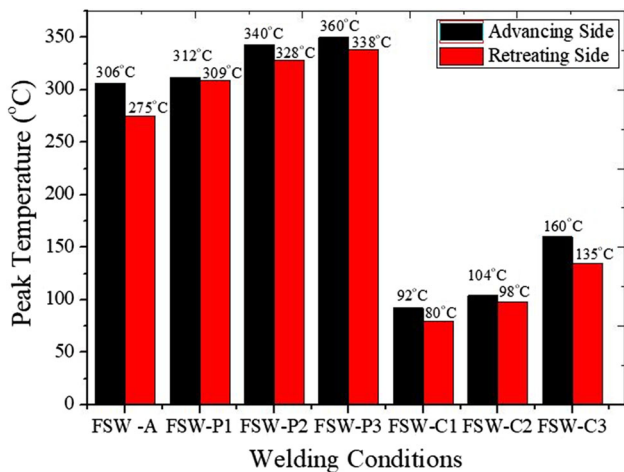
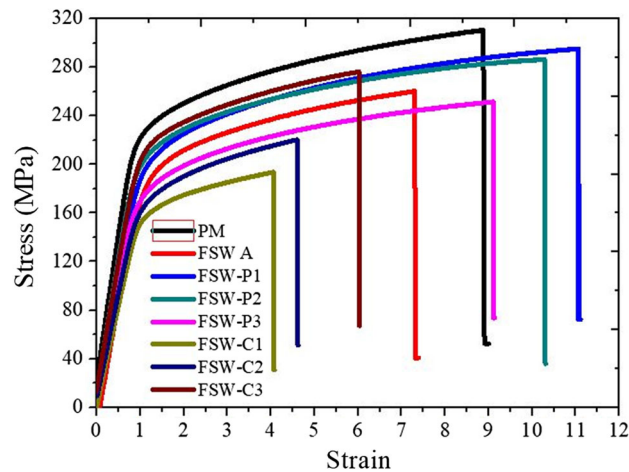Fig. 5 Comparison between peak temperatures of different welding conditions

Fig. 7 Stress vs. strain curve

Table 2 Experimental results

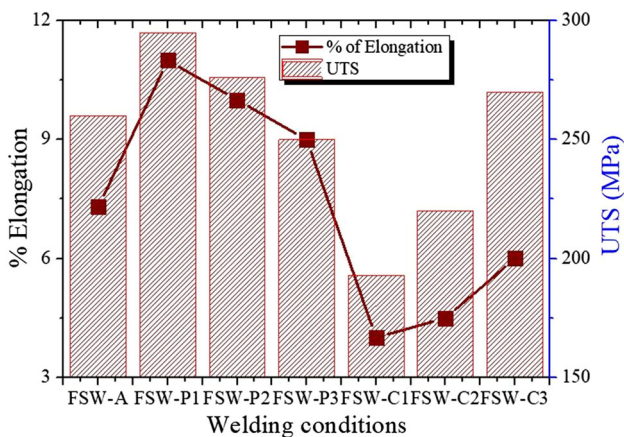|		Welding conditions						
Responses	Base metal	FSW-A	FSW-P1	FSW-P2	FSW-P3	FSW- C1	FSW-C2	FSW-C3
UTS, MPa	310	260	295	276	250	193	220	270
% changes in UTS			13.5 (+)	6 (+)	3.84 (−)	25 (−)	15 (−)	4 (+)
% of elongation	9	7.3	11	10	9	4	4.5	6
Hardness, HV (at nugget zone)	110	81.03	90	89	86	73.3	75	83
Grain size (microns)	7.9		5. 3					5.58

Fig. 6 UTS and percentage elongation under different welding conditions

Nevertheless, if the cooling rate is high then it causes improper heat generation during the process. Input heat directly affects the joint properties. Thus, proper water cooling is required for obtaining better mechanical and metallurgical properties. In present study, the joint strength is increased by 4% over FSW-A when water temperature is 65 °C. Although it is decreased by 25% and 15% than FSW-A when water temperatures are 22 °C and 2 °C respectively. This phenomenon can be explained as follow: water cooling decreases the recrystallization temperature of NZ and thus controls the dissolution of strengthening

particles. However, at high cooling rate, the necessary heat input during the process is reduced causing improper mixing of materials. It results in degradation of mechanical strength of the joint.

The percentage elongation of specimens obtained by different welding conditions is presented in Fig. 6. It is obvious from Fig. 6 that percentage elongation is 7.3 for FSW-A; 11, 10, and 9 for FSW-P1, FSW-P2, and FSW-P3, respectively; and 4, 4.5, and 6 for FSW-C1, FSW-C2, and FSW-C3, respectively. Joint fabricated under preheating conditions shows comparatively higher percentage elongation. This is owing to appropriate mixing of material and natural aging due to presence of additional heat. In case of water cooling, the percentage elongation is minimum. It is attributed to faster cooling rate and insufficient amount of heat during the process, resulting in improper mixing of material. It is also observed that in case of water cooling percentage elongation increases with decrease in cooling rate (i.e., ice water cooling to hot water cooling).

3.3 Microhardness Testing

Microhardness variation in 6xxx series is interrelated with grain size, density of precipitates, movements of dislocations, and dispersal of strengthening precipitates. Intense heat and plastic deformation in NZ decrease the grain size of NZ than TMAZ and HAZ. Hence, it is observed that NZ has higher microhardness than near about region. This is in accordance with the equation given by Hall–Petch (Ref 19). Rajakumar et al. (Ref 20) reported that higher hardness value of NZ is attributed to higher density of dispersal precipitates that

resulted by precipitation hardening due to natural aging during the process. Figure 8 shows the microhardness distribution for simple FSW, FSW with preheating, and FSW with water cooling. The microhardness of parent metal is found as 115 HV. It is observed that for all the experimental conditions microhardness of parent metal is higher than NZ. It is because of softening of NZ resulting in degradation of hardness behavior. This finding is in line with finding of past research works (Ref 21-23). The softening of NZ occurs owing to coarsening and dissolution of strengthening precipitates. These precipitates completely depend upon thermal cycle of FSW. Microhardness value of RS is observed higher than AS. This is attributed to higher temperature of AS (as shown in Fig. 4) leading toward termination of strengthening precipitates. In current study, it is evident that preheating conditions show better microhardness value of NZ. In case of preheating, owing to material softening, generation of frictional heat is less as compared to FSW-A. This helps in reduction in dissolution of precipitates and thus enhancement of microhardness. On the other hand, in case of water cooling condition, maximum microhardness value of NZ is obtained for FSW-C3 condition; followed by FSW-C2, FSW-C1. The reason is improper heat generation owing to rapid cooling during normal and cold-water conditions.
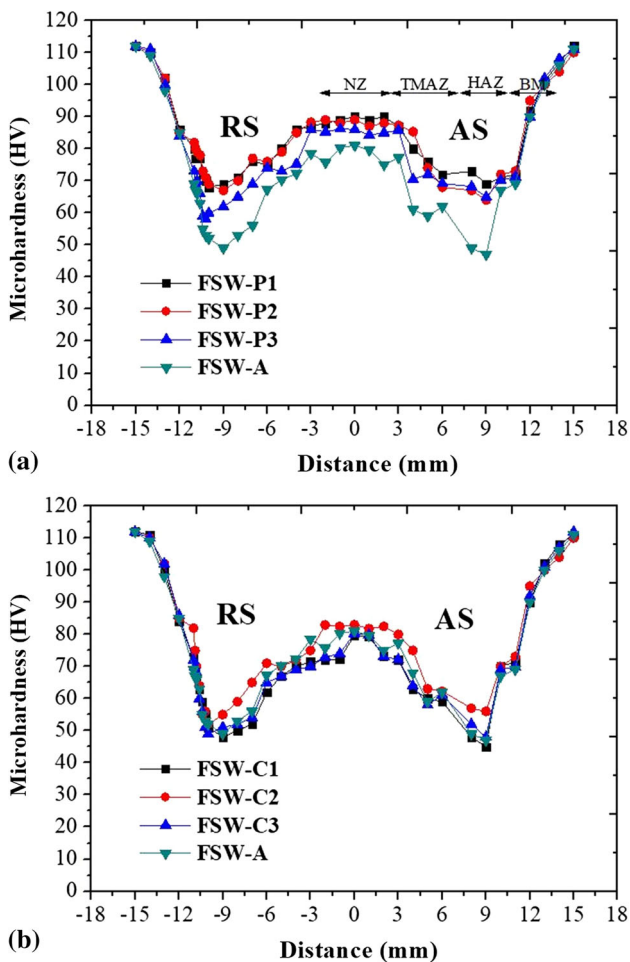
3.4 Macrostructural Analysis

The FSW-A, FSW-P1, and FSW-C3 specimens have been analyzed by optical microscope for macrostructural analysis as shown in Fig. 9. The macrostructure morphology of FSW joint is classified by three distinct zones: nugget zone or stir zone (NZ or SZ), thermomechanical affected zone (TMAZ), and heat-affected zone (HAZ). A line is clearly visible in macrograph of FSW-P1 that divides these three distinct zones; designated as fusion line. The grains in HAZ are elongated and
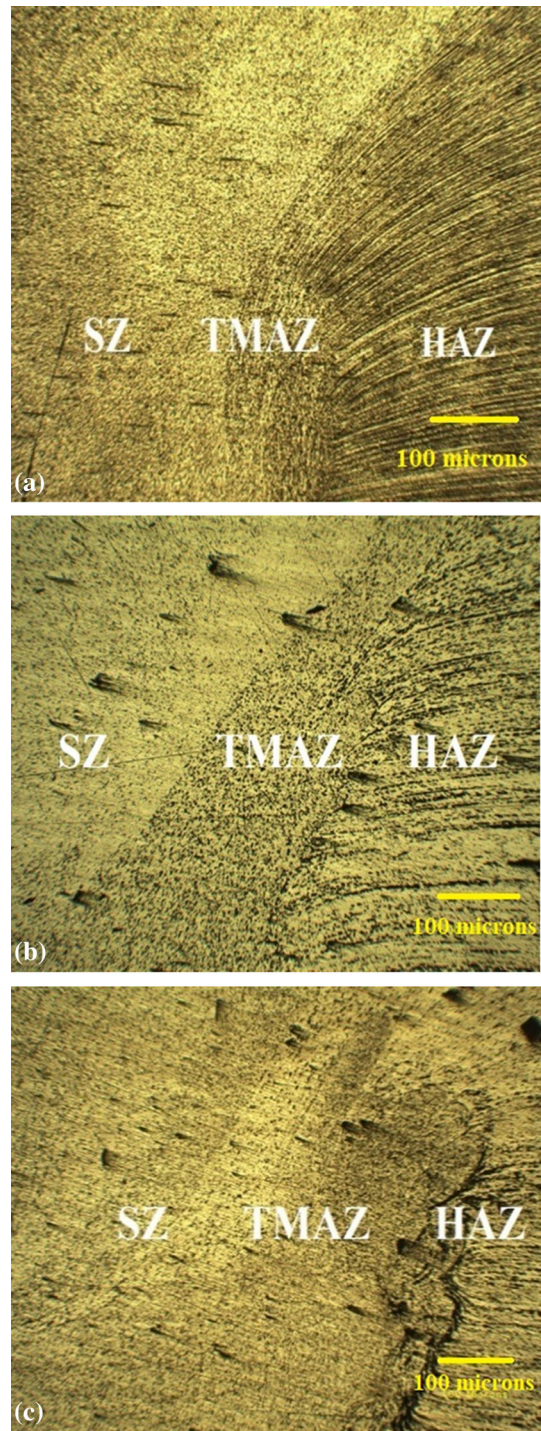

Fig. 8 (a) Microhardness distribution (a) preheating; (b) water cooling

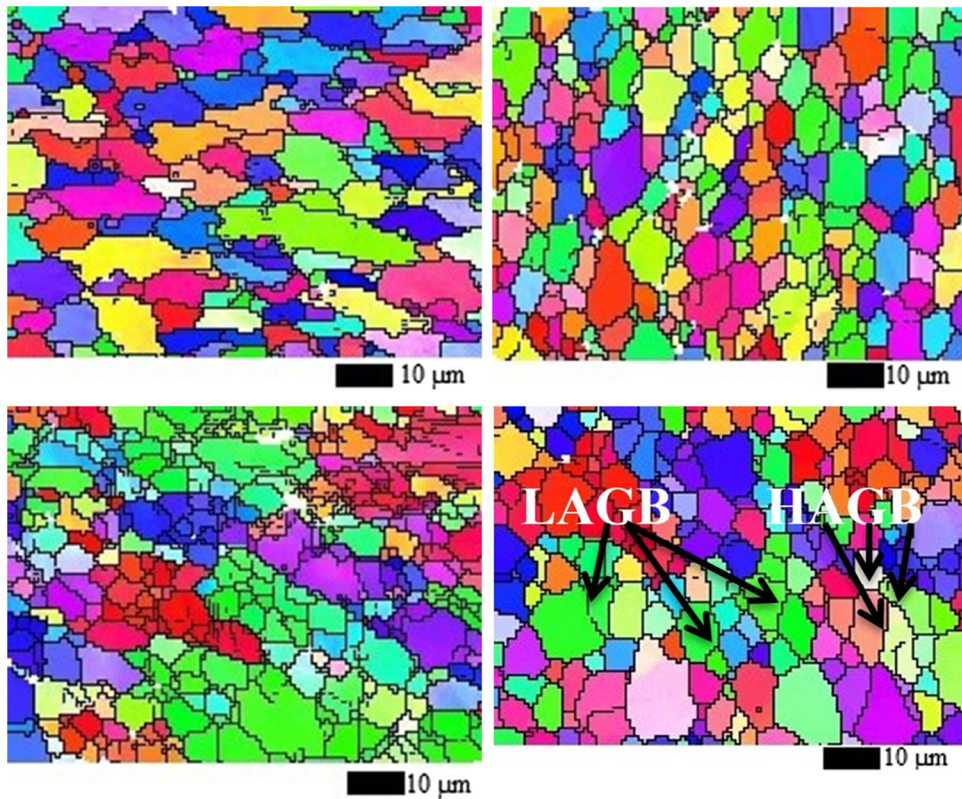**Fig. 9** Macrostructure of specimen for (a) FSW-A; (b) FSW-P1; (c) FSW-C3

Fig. 10 EBSD analysis of (a) parent metal, (b) FSW-A; (c) FSW-P1; and (d) FSW-C3
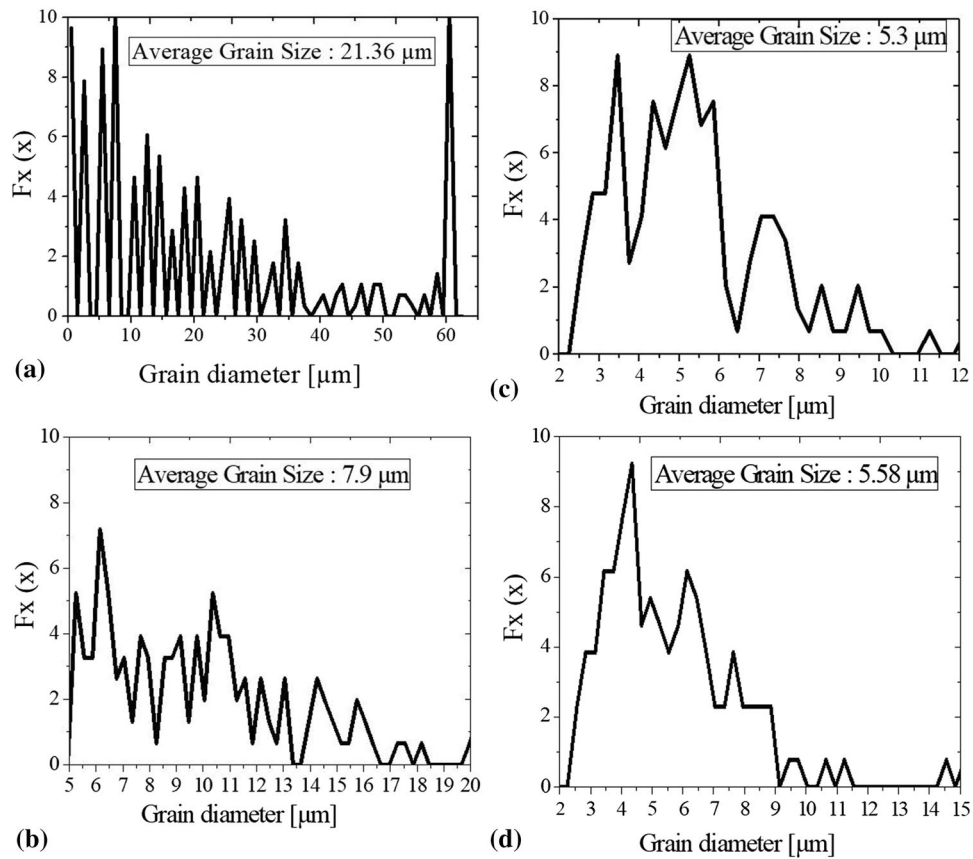

Fig. 11 Grain-size distribution of (a) base metal, (b) FSW-A; (c) FSW-P1; (d) FSW-C3

bent, whereas fine grains are observed in SZ. TMAZ is varied for every experiment and measured in the range of variation of 1-2.5 mm. It is obvious that preheating and water cooling does not affect the final shape of weld zone. In case of FSW-P1, higher degree of deformation occurs in SZ. The reason is formation of fine recrystallized grain structure as compared to FSW-A and FSW-C3. In FSW-C3, finer grains are observed as compared to FSW-A. This owing to decrease in heat input leads to refinement of grains. This finding is in resemblance with the finding of Lui et al. (Ref 24).

3.5 Microstructural/EBSD Analysis

Microstructural analysis of parent metal, and NZ of FSW-A, FSW-P1 *(highest strength specimen of preheating condition)*, and FSW-C3 *(highest strength specimen of water cooling condition)* has been executed by SEM with EBSD attachment as shown in Fig. 10. It is apparent that parent metal consists of large elongated grains as compared to FSW joints. High-angle grain boundaries (HAGB) and low-angle grain boundaries (LAGB) are observed in Fig. 9. HAGB represents different grains, and LAGB represents the same colored grains with separate boundary. Comparatively, finer equiaxed grains are observed in NZ of FSW joints than parent metal owing to dynamic recrystallization in NZ. Figure 11 presents the grain-size distribution of parent metal, and NZ of FSW-A, FSW-P1, and FSW-C3. The average grain sizes in all the cases are also depicted in Fig. 10. It is evident that average grain size of parent metal is 21.3 μm, while average grain size of NZ of FSW-A, FSW-P1, and FSW-C3 is 7.9, 5.3, and 5.58 μm, respectively. The variation in grain size of NZ is attributed to variation in heat input during the process. This is in accordance with finding of Sharma et al. (Ref 25). This variation in grain size can be conceptually explained by misorientation map of NZ of FSW joints. Figure 12 depicts the misorientation map of NZ for FSW-A, FSW-P1, and FSW-C3. It is apparent that the average misorientation angle of NZ of FSW-A is 14°, while it is 28.3° and 22.5° for FSW-P1 and FSW-C3, respectively. Higher misorientation angle reflects higher value of deformation and smaller grain size. The credential of this observation can also be scrutinized by strength and percentage elongation obtained for different joints (Table 2).

3.6 Texture Analysis

Figure 13(a) represents the texture of base material that shows the typical rolling texture of fcc metals. The texture at NZ for normal, preheating, and water cooling conditions is shown in Fig. 13(b), (c), and (d). Figure 13(b) textures consist of fiber of simple shear texture represented by green. This is an indication of plastic flow in NZ vigorously begin due to presence of shear stress along the pin surface. Figure 13(c) and (d) shows the texture surface under preheating and water cooling conditions. Both textures show the presence of fiber of simple shear texture same as of FSW-A, but rotated from the ideal shear axis. This is attributed toward the formation of fine grains in the NZ without highly alteration of the NZ texture (Ref 26, 27).

Figure 14 shows the x-ray diffraction (XRD) pattern of FSW welded sample under different welding conditions. Each XRD plot consists of five major peaks at an angle of 38.47°, 44.7°, 65.4°, 78.6°, and 82.7°, respectively, with corresponding planes of reflection are (111), (200), (220), (311), and (222). These peaks are recognized as aluminum peaks

(*JCPDS#040787*). There is also one peak observed in each XRD graph at angle of 40.6° with corresponding planes of (220). These peaks are identified as Mg_2Si (*JCPDS#650690*). It is clearly visible in Fig. 13 that both aluminum and strengthening precipitates peaks are present on XRD plot. It is the indication of formation and dissolution of strengthening precipitates during the FSW process under different welding conditions.
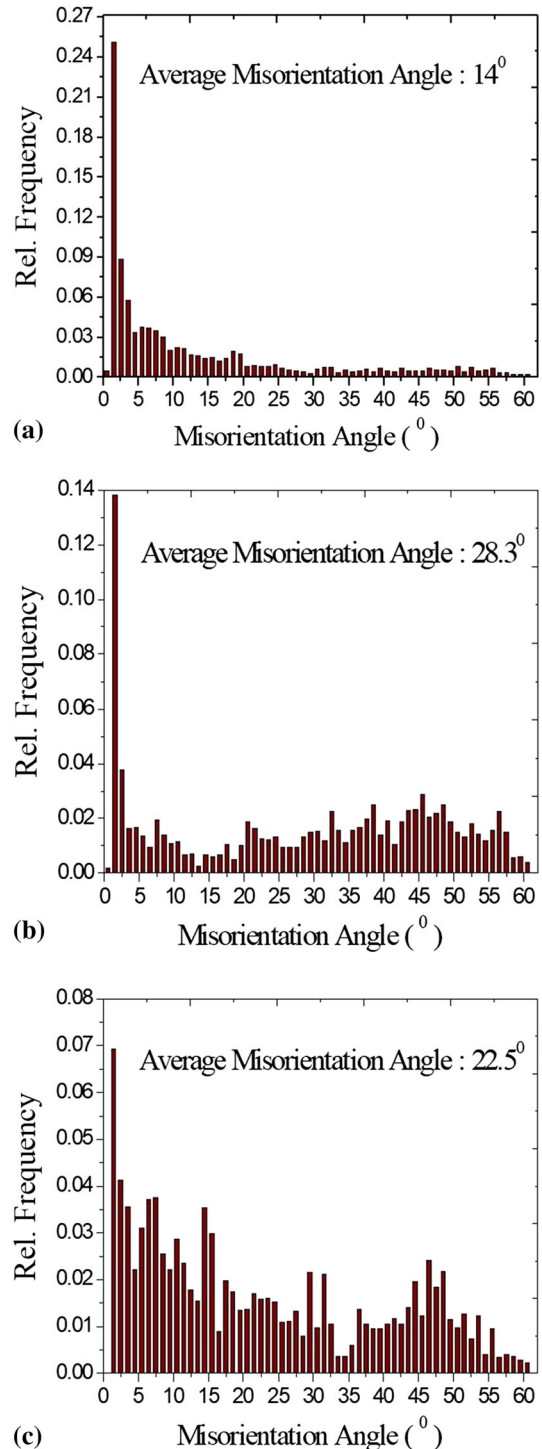

(a)

(b)

(c)

Fig. 12 Histogram showing misorientation angle of (a) FSW-A; (b) FSW-P1; and (c) FSW-C3

3.7 Fractography

The tensile fracture surface of FSW-A, FSW-P1 (*highest strength specimen of preheating condition*), and FSW-C3 (*highest strength specimen of water cooling condition*) is analyzed using SEM and illustrated by Fig. 15. The fracture surface provides information regarding microstructural characteristics that affect the mechanical properties of the joint. It is observed that all the fracture surfaces consist of dimples; reflects ductile nature of fracture. It is evident from Fig. 15(a) that small and deep dimples with torn edges are present on fracture surface of FSW-A joint. In contrast, larger and shallow dimples are observed on the fracture surface of FSW-P1 as shown in Fig. 15(b). It indicates higher plastic deformation and ductility in case of FSW-P1 joint. This observation is also established by respective percentage elongation and misorientation angle as shown in Fig. 6 and 12, respectively. On the other hand, deep and small circular and parabolic dimples are observed on fracture surface of FSW-C3. Parabolic dimples are indication of shear fracture with fibrous pullout. This reflects higher deformation with decrement in ductility. It is also confirmed by percentage elongation and misorientation angle. In addition, presence of large number of second-phase particles observed in FSW-C3 fracture surface indicates higher tensile strength with less ductility.

4. Conclusions

In this manuscript, the effects of preheating and water cooling on thermal, mechanical, and metallurgical properties of FSW joint have been discussed. It is observed that fabricated joints are free from tunnel defect indicating the proper design of fixture and adapting of appropriate experimental technique. From the current study, following conclusions can be drawn.

- Thermal analysis shows that the initial temperature is higher in case of preheating than other welding conditions. In case of water cooling, the temperature is suddenly dropped after processing time. It is attributed to the combined effect of water cooling and lack of frictional heat input after processing time. Moreover, the temperature on AS is higher for all welding conditions.
- Joints fabricated at preheating condition of 100 and 125 °C have joint strength of 295 and 276 MPa, respectively; 13.5 and 6% higher strength than FSW joint obtained at atmospheric condition. This is owing to proper mixing of material in NZ and natural aging. This is happed due to preheating the material before welding.
- The joint fabricated at hot water cooling condition has 4% higher strength than joint fabricated at atmospheric condi-
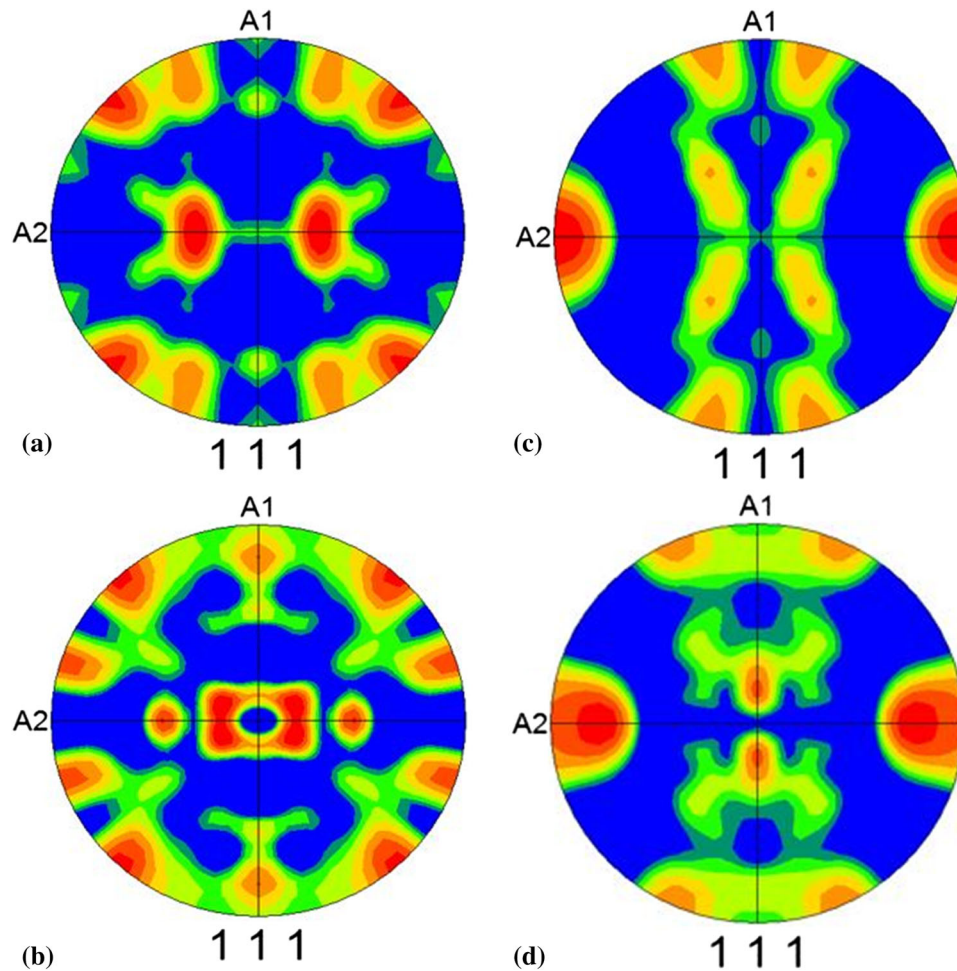

Fig. 13 {1 1 1} pole figure of FSW samples (a) parent metal; (b) FSW-A; (c) FSW-P1; (d) FSW-C3
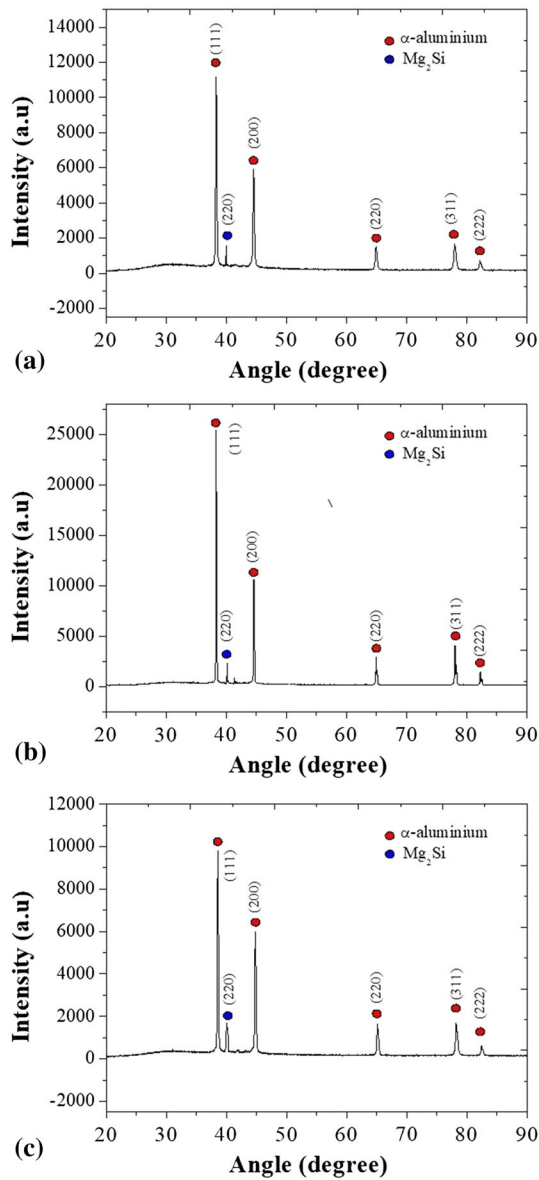
Fig. 14 X-ray diffraction of FSW joint of AA6082 (a) FSW-A; (b) FSW-P1; (c) FSW-C3

tion. This strength is decreased with decrease in the temperature of water. The higher strength is obtained due to presence of fine grains in NZ.

- Preheating has more impact on microhardness and ductility of the joint as compared to FSW-A and FSW-C conditions.
- The EBSD analysis shows that the grain size of the parent metal, under atmospheric condition, preheating at 100 °C, and water cooling condition of 65 °C are 21.3, 7.91, 5.3, and 5.6 μm, respectively.
- FSW provided shear texture in the NZ with main component of fiber. It is observed that texture for preheating and water cooling rotated about ideal shear axis as compared to normal welding condition. This results in the formation of finer grains in NZ.
- Round-shaped and high-density dimples are observed on fracture surface of joints obtained at preheating condition of 100 °C, whereas less deep dimples are observed on
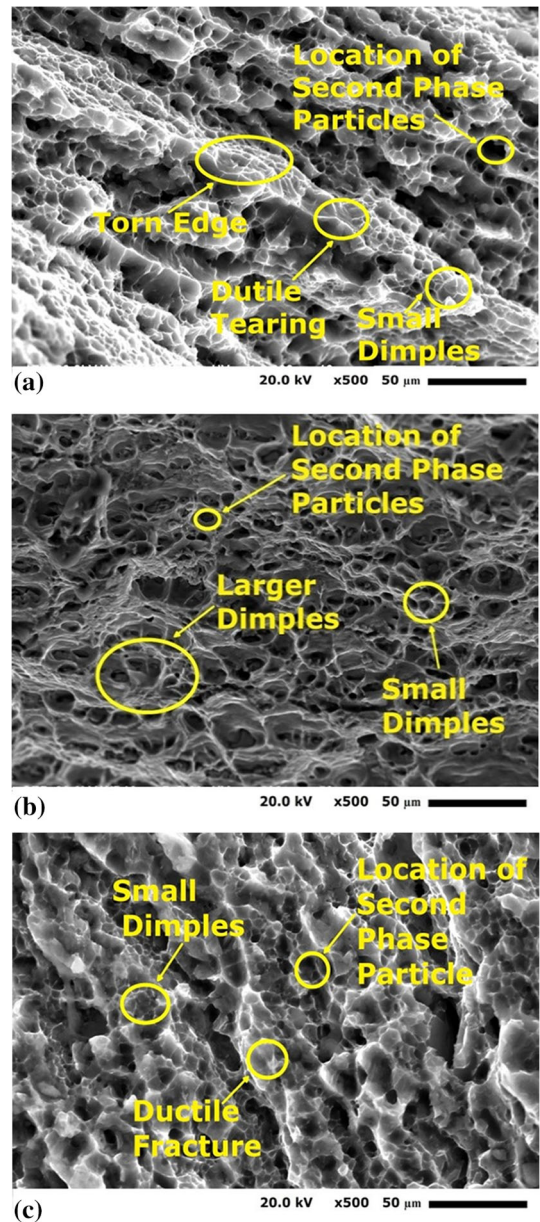

Fig. 15 Fracture surface of tensile specimen of (a) FSW-A; (b) FSW-P1; and (c) FSW-C3

water cooling condition of 65 °C and atmospheric condition. Parabolic dimples are observed on fracture surface of joint fabricated under water cooling of 65 °C. This leads to reduction in ductility and resulting in shear fracture.

Acknowledgments

References

1. A.K. Lakshminarayanan and V. Balasubramanian, Process Parameters Optimization for Friction Stir Welding of RDE-40 Aluminium Alloy

Using Taguchi Technique, *Trans. Nonferrous Met. Soc. China*, 2008, **18**(3), p 548–554

2. S. Verma and J. Misra, *A critical review of friction stir welding process*, DAAAM International Scientific Book, Vienna, 2015, p 249–266

3. S. Verma, M. Gupta, and J.P. Misra, Friction Stir Welding of Aerospace Materials: A State of Art Review, *Chapter*, 2016, **13**, p 135–150

4. D. Lohwasser and Z. Chen, *Friction stir welding: from basics to applications*, Woodhead Publishing Limited, New Delhi, 2010

5. H.I. Dawood, K.S. Mohammed, A. Rahmat, and M.B. Uday, Effect of Small Tool Pin Profiles on Microstructures and Mechanical Properties of 6061 Aluminum Alloy by Friction Stir Welding, *Trans. Nonferrous Met. Soc. China*, 2015, **25**(9), p 2856–2865

6. L. Trueba, Jr., G. Heredia, D. Rybicki, and L.B. Johannes, Effect of Tool Shoulder Features on Defects and Tensile Properties of Friction Stir Welded Aluminum 6061-T6, *J. Mater. Process. Technol.*, 2015, **219**, p 271–277

7. A. Heidarzadeh, H. Khodaverdizadeh, A. Mahmoudi, and A.E. Nazari, Tensile Behavior of Friction Stir Welded AA 6061-T4 Aluminum Alloy Joints, *Mater. Des.*, 2012, **37**, p 166–173

8. P. Cavaliere, A. Squillace, and F. Panella, Effect of Welding Parameters on Mechanical and Microstructural Properties of AA6082 Joints Produced by Friction Stir Welding, *J. Mater. Process. Technol.*, 2008, **200**(1–3), p 364–372

9. S. Gopi and K. Manonmani, Influence of Shoulder Profile and Shoulder Penetration on Joint Strength; of Friction Stir Welded AA6082 in Conventional Milling Machine, *Eur. J. Sci. Res.*, 2012, **73**(1), p 20–32

10. P.C. Sinclair, W.R. Longhurst, C.D. Cox, D.H. Lammlein, M. Alvin, and G.E. Cook, Materials and Manufacturing Processes Heated Friction Stir Welding: An Experimental and Theoretical Investigation into How Preheating Influences Process Forces Heated Friction Stir Welding: An Experimental and Theoretical Investigation into How Preheating Influences Process Forces, *Mater. Manuf. Process.*, 2010, **25**, p 4–37

11. S. Verma and J.P. Misra, Study on Temperature Distribution During Friction Stir Welding of 6082 Aluminum Alloy, *Mater. Today Proc.*, 2017, **4**(2), p 1350–1356

12. D. K. Yaduwanshi, S. Bag and S. Pal. Effect of preheating in hybrid friction stir welded dissimilar joint. in *Design and Research Conference*, 165-1-165-6 (2014)

13. A.O. Zargar and H. Kukatpally, The Preheating Influence on Welded Joint Mechanical Properties Prepared by Friction Stir Welding Aluminum Alloy H20-H20, *Middle-East J. Sci. Res.*, 2013, **15**, p 1415–1419

14. P.M. Kavalco, L.C. Canale, and G.E. Totten, Quenching of Aluminum Alloys: cooling Rate, Strength, and Integranular Corrosion, *Heat Treat. Prog.*, 2009, **9**(7), p 25–30

15. H.J. Liu, H.J. Zhang, Y.X. Huang, and Y.U. Lei, Mechanical Properties of Underwater Friction Stir Welded 2219 Aluminum Alloy, *Trans. Nonferrous Met. Soc. China*, 2010, **20**(8), p 1387–1391

16. S. Verma, M. Gupta, and J. P. Misra. Study of thermal cycle, mechanical, and metallurgical properties of friction stir welded aviation grade aluminum alloy. in *Proceedings of the Institution of Mechanical Engineers, Part G: Journal of Aerospace Engineering*, p. 0954410018816601 (2018)

17. D.C. Hofmann and K.S. Vecchio, Submerged Friction Stir Processing (SFSP): An Improved Method for Creating Ultra-Fine-Grained Bulk Materials, *Mater. Sci. Eng. A*, 2005, **402**(1), p 234–241

18. H. J. Liu, N. Guo and J. C. Feng. Friction stir welding assisted by micro-plasma arc. in *Proceedings of the 6th International Symposium on Friction Stir Welding, Montreal* (2006)

19. W. Xunhong and W. Kuaishe, Microstructure and Properties of Friction Stir Butt-Welded AZ31 Magnesium Alloy, *Mater. Sci. Eng. A*, 2006, **431**(1), p 114–117

20. S. Rajakumar, C. Muralidharan, and V. Balasubraminian, Predicting Tensile Strength, Hardness and Corrosion Rate of Friction Stir Welded AA6061-T6 Aluminium Alloy Joints, *Mater. Des.*, 2011, **32**, p 2878–2890

21. Y.M. Hwang, Z.W. Kang, Y.C. Chiou, and H.H. Hsu, Experimental Study on Temperature Distributions Within the Workpiece During Friction Stir Welding of Aluminum Alloys, *Int. J. Mach. Tools Manuf.*, 2008, **48**(7–8), p 778–787

22. Y.S. Sato, M. Urata, and H. Kokawa, Parameters Controlling Microstructure and Hardness During Friction-Stir Welding of Precipitation-Hardenable Aluminum Alloy 6063, *Metall. Mater. Trans. A*, 2002, **33**(3), p 625–635

23. S. Verma, M. Gupta, and J.P. Misra, Optimization of Process Parameters in Friction Stir Welding of Armor-Marine Grade Aluminium Alloy Using Desirability Approach, *Mater. Res. Express*, 2018, **6**(2), p 026505

24. H.J. Liu, H.J. Zhang, and L. Yu, Effect of Welding Speed on Microstructures and Mechanical Properties of Underwater Friction Stir Welded 2219 Aluminum Alloy, *Mater. Des.*, 2011, **32**(3), p 1548–1553

25. C. Sharma, D.K. Dwivedi, and P. Kumar, Influence of In-Process Cooling on Tensile Behaviour of Friction Stir Welded Joints of AA7039, *Mater. Sci. Eng. A*, 2012, **556**, p 479–487

26. K.J. Al-Fadhalah, A.I. Almazrouee, and A.S. Aloraier, Microstructure and Mechanical Properties of Multi-Pass Friction Stir Processed Aluminum Alloy 6063, *Mater. Des.*, 2014, **53**, p 550–560

27. Y.S. Sato, H. Kokawa, K. Ikeda, M. Enomoto, T. Hashimoto, and S. Jogan, Microtexture in the Friction-Stir Weld of an Aluminum Alloy, *Metall. Mater. Trans. A*, 2001, **32**(4), p 941–948